Nuclear Instruments and Methods in Physics Research B 366 (2016) 6–12

Contents lists available at ScienceDirect

Nuclear Instruments and Methods in Physics Research B

journal homepage: www.elsevier.com/locate/nimb

A model dielectric function for low and very high momentum transfer

Maarten Vos

Atomic and Molecular Physics Laboratories, Research School of Physics and Engineering, The Australian National University, Canberra 0200, Australia

ARTICLE INFO

Article history:
Received 22 July 2015
Received in revised form 25 September 2015
Accepted 30 September 2015

Keywords:
Reflection electron energy loss spectroscopy
Mermin dielectric function
Compton profile

ABSTRACT

A model dielectric function is derived for TiO_2 based on reflection electron energy loss spectroscopy data and photoabsorption cross sections. The model is based on a set of Mermin oscillators. The input data is dominated by excitations at low momentum transfer, i.e. near the optical limit. Surprisingly the dielectric function derived at low momentum transfer describes the Compton profile quite well, while approaches based on Drude oscillators fail dramatically. The link between the dielectric function in the high-momentum transfer limit and a Compton profile is discussed. The underlying reason why the Mermin approach, which is based on a free electron model, is successful in describing the Compton profile is tentatively discussed.

1. Introduction

There is a lot of interest recently in methods to obtain the dielectric function $\epsilon(\boldsymbol{q},\omega)$ (with $\boldsymbol{q}$ the momentum transfer and ω the energy loss) of materials over an extended range of energy and momentum [1–4]. These quantities are the basis for the calculations of the inelastic mean free path of electrons and the stopping power of fast ions in matter. More generally the dielectric function is an essential ingredient of the description of electron–electron correlation in matter. Extraction of the dielectric function based on reflection electron energy loss spectroscopy(REELS) is usually based on extended Drude or Drude–Lindhard (D–L) models [5,6]. In its simplest form this approach does not give any broadening of the loss function (described by $\mathrm{Im}[-1/\epsilon(\mathbf{q},\omega)]$) with increasing momentum transfer, in clear contrast to experiment [7,8]. Agreement with the experiment can be improved by introducing a q-dependent broadening term [9,10].

This restriction is not present in the Mermin loss function [11]. It is based on a free-electron model and the width of the loss feature depends on $\mathbf{q}$, while maintaining the Bethe (or the related Tho mas–Reiche–Kuhn) sum rule for all $\boldsymbol{q}$ as well as the Kramers–Kronig sum rule. These desirable properties made the Mermin description of the valence band dielectric function the basis for the determination of the stopping of ions in matter [12].

A scattering electron interacts coherently over a distance of the order of $1/q$. At small momentum transfer the scattered electron interacts thus with a rather large volume of the target and one probes long-range density fluctuations (plasmons). At very large momentum transfer the projectile interacts coherently only with a small volume, containing only a single electron. In that case one can describe the interaction as a binary collision of the projectile and a target electron. The loss function at these large q values is usually referred to as the 'Bethe ridge'. Here the loss function reveals information about the target electron momentum distribution and can be considered a Compton profile [13]. In this paper we aim at obtaining a simultaneous description of both limiting conditions with a single dielectric function.

For a free electron gas, Lindhard derived a dielectric function that described both the collective behaviour at small q values and the single-particle excitations at large q values. The Mermin dielectric function is an extension of the Lindhard dielectric function that allows for a finite width of the peak in the loss function due to collective excitations at low q. There are several approaches to derive a dielectric function when the free electron approximation does not apply, e.g. by Penn [14] and Ashley [15], and a comparison of different approaches is given in Refs. [16,17].

In recent days it has become popular to describe the loss function of a wide range of materials by a sum of Mermin loss functions for small q excitations. A rigorous justification for the use of a sum of Mermin loss functions for materials that are far from free-electron like is usually not given. The heart of this paper is the investigation to what extent such an approach can still give a reasonable description of the loss function at both low and high q values.

In the next section we will revisit some of the properties of the Mermin loss function using the simple case of a carbon film as an example and demonstrate that both a more traditional electron energy loss spectrum and a Compton profile can be described in

E-mail address: maarten.vos@anu.edu.au

http://dx.doi.org/10.1016/j.nimb.2015.09.091
0168-583X/

a uniform way by the Mermin loss function. Subsequently, we investigate more quantitatively, using TiO_2 as a test case, if we can obtain a set of Mermin oscillators that simultaneously describes the feature-rich spectrum of a reflection electron energy loss spectroscopy (REELS) measurement (extended to higher energy loss values by photo-absorption measurements) as well as its Compton profile. Moreover the obtained dielectric function is in agreement simultaneously with the Bethe and Kramers–Kronig sum rules. Finally it is discussed if the reasonable agreement obtained can be understood in terms of some kind of a 'local density approximation'.

2. A simple illustration for carbon films

First let us introduce the topic considering the experimental results for a very thin (35 Å thick) free-standing carbon film. Two scattering measurements were done with the same electron spectrometer employing very different kinematical conditions [18,19]. The experiment was done in a transmission geometry and is shown schematically in Fig. 1, the scattering angle Θ_s was ≈45°.

In the first experiment the incoming electron energy was 25 keV, and outgoing electrons with an energy loss up to 100 eV were detected. The obtained spectrum is shown in Fig. 2(A). It shows a sharp peak near zero energy loss (the elastic peak, due to electrons deflected from a nucleus), and a broader, less intense feature at larger energy loss. The latter is due to electrons that created an electronic excitation in the film. The maximum momentum of an electronic excitation created under these conditions is much smaller than the momentum required to deflect a 25 keV electron over 45°. Therefore there are no projectile electrons scattered directly into the analyser by such an electronic excitation. All the detected electrons have scattered elastically from a nucleus as well. The situation is as in a normal REELS experiment [20]. The inelastic mean free path (IMFP) of a 25 keV electron in graphite is ≈270 Å [21]. Under these conditions (film thickness much smaller than the IMFP) the probability for multiple inelastic excitations is small and the shape of the loss part of the spectrum can be directly compared to the shape of the DIIMP (differential inelastic inverse mean free path). The (bulk) DIIMP $W_b(\omega, E_0)$ is related to the dielectric function by:

$$W_b(\omega, E_0) = \frac{1}{\pi E_0}\int_{q_-}^{q_+}\frac{dq}{q}\mathrm{Im}\left[\frac{-1}{\varepsilon(q,\omega)}\right] \quad (1)$$

with the limits of integration given by: $q_\pm = \sqrt{2mE_0} \pm \sqrt{2m(E_0-\omega)}$ [20].

To model $\mathrm{Im}[-1/\varepsilon(\boldsymbol{q},\omega)]$ one can use either a D–L oscillator with 3 parameters, ω_p (plasmon energy at $q=0$), γ (width of this plasmon) and α (dispersion of the loss feature with q):

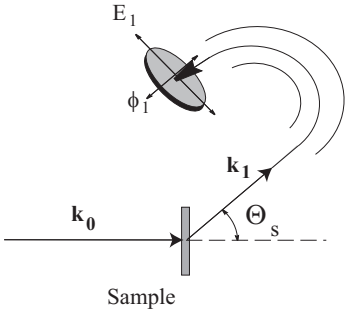

Fig. 1. A schematic view of the carbon film measurement done in a transmission geometry. The scattering angle Θ_s is 45°, $\mathbf{k}_0$ and $\mathbf{k}$ are the momentum of the incoming and detected electron respectively. The analyser resolves both the energy E_1 and azimuthal angle ϕ_1 of the detected electron.

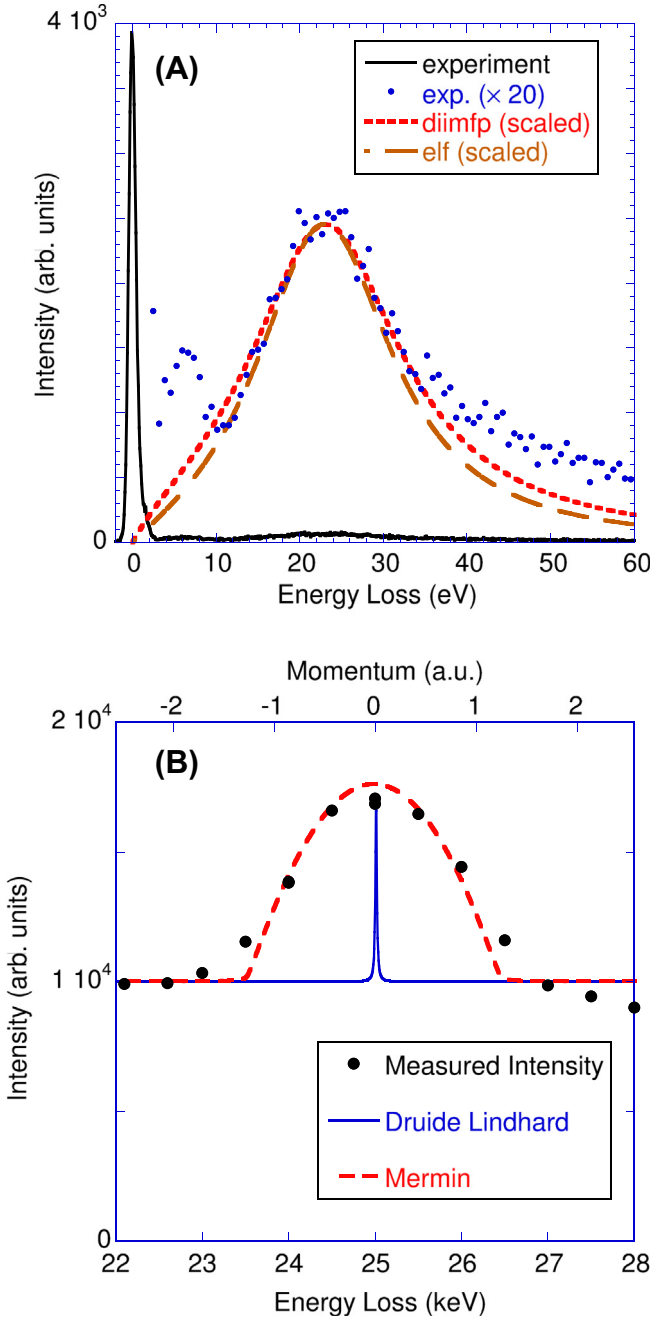

Fig. 2. (A) shows the energy loss spectrum for a 35 Å thick carbon film. The incoming energy was 25 keV. The shape of the loss spectrum can be described by the DIIMFP of a single Mermin oscillator centred at an energy loss of 25 eV and a width γ of 20 eV. The shape of the DIIMFP (short dashed line) is very close to the shape of the energy loss function $\mathrm{Im}[-1/\epsilon(q=0,\omega)]$ (ELF, long dashed line). A D–L based dielectric function with the same parameters has a very similar DIIMFP. In (B) the incoming energy was 50 keV and the spectrum was measured near $\omega = 25$ keV. The shape of this spectrum resembles $1/\epsilon(q=42.9,\omega)$ for the Mermin loss function, superimposed on a rather constant background. In contrast the width of the D–L loss function at $q = 42.9$ a.u. is orders of magnitude smaller.

$$\mathrm{Im}\left[\frac{-1}{\varepsilon_{\mathrm{DL}}(\boldsymbol{q},\omega)}\right] = \frac{\gamma\omega_p^2\omega}{(\omega^2-\omega_q^2)^2+\gamma^2\omega^2}\Theta(\omega-E_{\mathrm{gap}}) \quad (2)$$

with $\omega_q = \omega_p + \alpha q^2$ and $\Theta(\omega - E_{\mathrm{gap}})$ the step function assuring that no excitations are possible within the bandgap of a semiconductor. Alternatively one can use a Mermin oscillator:

$$\varepsilon_{\mathrm{M}}(q,\omega) = 1 + \frac{(1+i\gamma\omega)[\epsilon_{\mathrm{L}}(q,\omega+i\gamma)-1]}{1+i\gamma/\omega[\epsilon_{\mathrm{L}}(q,\omega+i\gamma)-1]/[\epsilon_{\mathrm{L}}(q,0)-1]}\Theta(\omega-E_{\mathrm{gap}}) \quad (3)$$

with $\epsilon_L(q,\omega)$ the Lindhard dielectric function, see e.g. [12] for a more extensive description. The Mermin dielectric function has dispersion build-in and is defined by two parameters: ω_p, the plasmon energy and γ, the width of the plasmon at $q = 0$. Moreover for $q = 0$ the Mermin and D–L dielectric function with the same ω_p and γ coincide.

For $E_0 = 25$ keV, the shape of the DIIMFP is not too different from the loss function in the optical limit: $1/\epsilon(q = 0, \omega)$. The calculated DIIMFP, as shown here, was obtained using the SESINIPAC program [22,23] for $E_0 = 25$ keV and a reasonable description of the main feature was obtained with either a single Mermin or single D–L oscillator with $\omega = 25$ eV and $\gamma = 20$ eV (Fig. 2(A)). Such a very simple model describes the main feature of the experiment.

In the second experiment the incoming energy was increased to 50 keV, but the detected electron energy was kept near 25 keV. Fig. 2(B) shows the obtained spectrum. It has a broad peak near 25 keV energy loss. Under these conditions, one can detect projectiles that have *only* interacted with a target electron, as the momentum and energy transferred to a target electron now match the change in energy and momentum of the projectile. (In fact the particle detected here can either be considered the scattered projectile or the ejected target electron.) If the target electron was stationary before the collision, the laws of energy and momentum conservation dictate that the energy loss of a 50 keV electron after scattering over 45° is exactly 25 keV. The considerable width observed in the energy loss spectrum is due to the momentum distribution of the target electrons. The measurement is in fact a Compton profile of the target electron momentum distribution, as will be explained in Section 3. The Compton profile obtained here is on top of a rather constant background, presumably due to multiple scattering effects, but details here are not understood.

For our incoming energy this Compton profile is a cut through the Bethe ridge at $q = 42.9$ a.u. (For simplicity we neglect the small relativistic corrections throughout this paper, using the correct relativistic kinematics this momentum transfer would be 43.4 a.u. and the actual scattering angle was 44.3°.) In Fig. 2(B) the measurement is compared with $\mathrm{Im}[-1/\epsilon(q,\omega)]$ of the same Mermin dielectric function but now not near $q = 0$ but at $q = 42.8$ a.u. A constant is added to account for the multiple scattering background. Considering the crudeness of our loss function the agreement is very good. The D–L dielectric function with $\alpha = 1$ also gives a peak at 25 keV energy loss, but with a width of only 20 eV, 100 times too small.

Note that the width of the loss feature in the upper and lower panel of Fig. 2 differs by a factor of 100. However the simple one-oscillator Mermin model describes both measurements well. We want to explore this fact in some detail in the next section.

3. Relation between Compton profiles and the dielectric function

Under high momentum transfer conditions the incoming projectile interacts with a single target electron and the collision can be described as a collision between two free particles. From the laws of conservation of energy and momentum one can calculate the energy transferred from the projectile to a target electron with momentum $\boldsymbol{p}$. The energy loss ω of the projectile due to the scattering is given by:

$$\omega = \frac{q^2}{2m} + \frac{\boldsymbol{p}\cdot\boldsymbol{q}}{m} \tag{4}$$

with m the mass of the electron (equal to unity in atomic units) [13]. The energy transfer depends on p_q, the component of $\boldsymbol{p}$ along the momentum transfer direction. This makes it possible to plot the measured intensity as a function of p_q, as is done at the upper axis of Fig. 2(B). The intensity at a certain p_q value is proportional to the 'momentum density' i.e. the number of target electrons with the corresponding p_q value before the collision.

If one takes a second measurement at lower incoming energy, then the position of the peak in Fig. 2(B) would move to smaller energy loss values and the width of the peak would decrease. This is illustrated in Fig. 3(A). Transforming the energy loss axis into a momentum axis according to Eq. (4) results for both measurements in the same profile (except for a vertical scaling factor). This is illustrated in Fig. 3(B) and both measurements would provide the same information about the target electron momentum distribution. In reality such a profile is usually obtained by scattering of X-rays, rather than electrons and is referred to as (X-ray) Compton scattering. In that case one does not need ultra-thin films in order to prevent multiple scattering as the interaction of X-rays with the target is much weaker. The measurement of Compton profiles using electron beams has been explored for gas-phase target [24] and for very thin films in the electron microscope [25,26].

The Mermin dielectric function is an extension of the Lindhard dielectric function. Both are developed for the description of a free electron gas. The energy loss at small q values is related to the excitation of a collective mode in the electron gas (plasmon). The plasmon energy is related to the density of the electron gas:

$$\omega_p^2 = \frac{4\pi n e^2}{m} \tag{5}$$

with n the number of valence electrons per unit volume.

At large q the measured energy loss distribution is a Compton profile and its width depends on the momentum of the electrons present. For an electron gas the range in momentum space that is occupied is determined by the Fermi sphere radius, which again depends on the density of the electron gas:

$$k_f^3 = 3\pi^2 n \tag{6}$$

It is the beauty of the Mermin dielectric function that it describes both limiting cases with only two parameters (electron density and damping γ).

4. Dielectric function of TiO_2

One can write for the complex dielectric function $\epsilon = \epsilon_1 + i\epsilon_2$ with $\epsilon_{1,2}$ both real. In many cases, in particular transition metals and transition metal oxides, the energy loss spectrum is not dominated by a single plasmon, but shows several peaks. The loss function $\mathrm{Im}[-1/\epsilon(q,\omega)]$ is given by:

$$\mathrm{Im}[-1/\epsilon] = \frac{\epsilon_2}{\epsilon_1^2 + \epsilon_2^2} \tag{7}$$

Peaks in $\mathrm{Im}[-1/\epsilon(q,\omega,)]$ due to the fact that $\epsilon_1 = 0$ are due to collective excitations (plasmons). For feature-rich loss spectra the peaks are due to an interplay between ϵ_1 and ϵ_2.

It is customary to fit a more complex REELS with a set of oscillators, either of the D–L [5,6] or Mermin type [12]. The Mermin dielectric function is firmly based on a free electron model and the justification of the use of a sum of Mermin-type oscillators for the description of more complicated solids is not obvious. Now the ω_i value of oscillator i is not related in a straight forward way to the density of the target electrons. Is it still possible to describe the behaviour at low and high momentum transfer with a set of Mermin-type oscillators? We will take an empirical approach here and investigate for the case of TiO_2 if such an approach leads to meaningful results. The REELS experiment was described in Ref. [27]. It used a thick sample and an incoming energy of 40 keV. The spectra were corrected for multiple

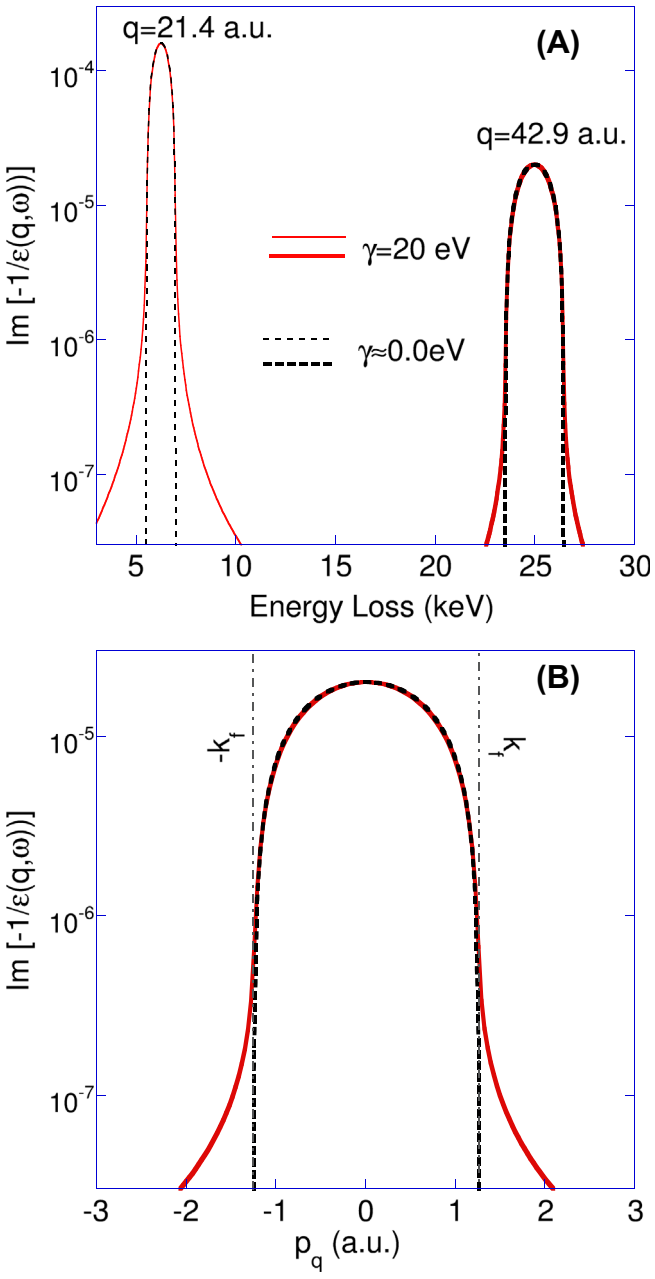

Fig. 3. In (A) the q dependence of $\mathrm{Im}[-1/\epsilon(q,\omega)]$ is shown under conditions when the impulse approximation applies for the same Mermin oscillator used in Fig. 2. At $q = 42.9$ a.u. (thick lines: full line $\gamma = 0$ eV dashed line $\gamma = 20$ eV) the peak is at 4× larger energy loss value, (and has double the width) compared to one calculated at 21.4 a.u. (thin lines). In (B) the same quantity is plotted for $q = 42.9$ as a function of p_q (using Eq. (4)). The value of k_f indicated is obtained using Eqs. (5) and (6). The effect of the damping γ is minor. The 21.4 a.u. line has exactly the same shape, when plotted as a function of p_q except for a scaling factor of 4.

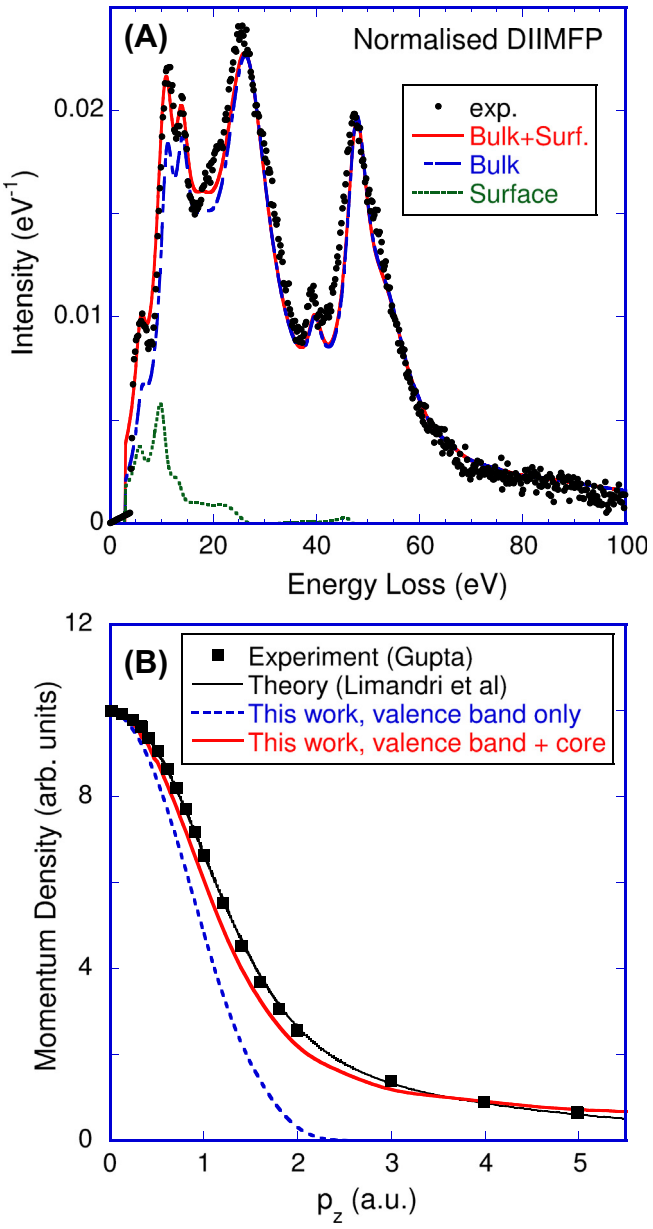

Fig. 4. (A) The spectrum of TiO_2 de-convoluted for multiple scattering according to [28]. The observed distribution is fitted with calculated DIIMFP based on a set of Mermin oscillators plus a small contribution due to surface excitations (red line). In (B) we compare the behaviour of the same set of Mermin Oscillators at high momentum transfer with a measured X-ray Compton profile (squares) as measured by Gupta [29] and the very similar computed Compton profile (thin solid black line) [32]. The dashed line uses Mermin oscillators for the valence band only, the full line is after inclusion of additional oscillators for the core levels. (For interpretation of the references to colour in this figure caption, the reader is referred to the web version of this article.)

scattering using the method of Ref. [28]. The resulting DIIMFP is shown in Fig. 4(A).

Unfortunately it is not possible to use electrons to measure its Compton profile as was done in Fig. 2(B) for carbon, as for heavier elements the multiple scattering background becomes even more severe. We can, however, use a X-ray Compton measurement to determine the shape of the dielectric function at high momentum transfer via Eq. (4). Such an X-ray Compton measurement was published by Gupta [29].

An established approach to the analysis of REELS measurements is the fitting of the single scattering distribution with a set of D–L oscillators, as can be done using the QUASUS/QUEELS software [30]. This approach was followed in Ref. [27] for TiO_2, and has the advantage that the surface excitations are taken into account on a quite sophisticated level but the influence of surface excitation is minor at the energy used here. Here we will follow a different approach based, introduced by Abril et al. [12] based on the sum of Mermin loss functions:

$$\mathrm{Im}\left[\frac{-1}{\epsilon(\boldsymbol{q},\omega)}\right] = \sum_i A_i \mathrm{Im}\left[\frac{-1}{\epsilon_{\mathrm{Mi}}(\boldsymbol{q},\omega)}\right] \tag{8}$$

and treating the small contributions of surface excitations in a more approximate way.

At these high energies the measured spectrum, after correcting for multiple scattering is close to $\mathrm{Im}[-1/\epsilon(\omega, \boldsymbol{q}=0)]$. In the optical limit the D–L and Mermin dielectric functions coincide, i.e. the parameters used in Ref. [27] were used as a first try for the description based on 9 Mermin oscillators but varied somewhat to improve the agreement with experiment. The resulting values are given by the first 9 oscillators in Table 1. The small contribution of surface excitations are taken into account based on the shape of the surface loss function and excitation probability (6% at 40 keV) as calculated using SESINIPAC.

The amplitude of the oscillators are set on an absolute scale by the Kramers–Kronig sum rule:

$$1 - \mathrm{Re}\left[\frac{1}{\epsilon(0,0)}\right] = 1 - \frac{1}{n^2} = \frac{2}{\pi}\int_0^\infty \mathrm{Im}\left[\frac{-1}{\epsilon(0,\omega)}\right]\frac{d\omega}{\omega} \qquad (9)$$

where in practise $1/\epsilon(0,0)$ is calculated from the refractive index n at a photon energy of the order of the experimental resolution [31].

Subsequently we calculate the shape of $\mathrm{Im}[-1/\epsilon(\omega,\ q)]$ at high momentum, and the shape of the Compton profile using Eq. (4). Here the choice of q value does not really matter as long as it is large enough for the impulse approximation to be valid, e.g. larger than 10 a.u. The obtained result was convoluted with the experimental resolution of the Compton profile (0.55 a.u.). The comparison is done in Fig. 4.

The agreement between the calculated profile (dashed line in Fig. 4) and the experimental Compton profile is limited, as the latter drops off much more slowly for large p_q values. This is due to a significant contribution of core electrons to the Compton profile. These electrons have a broad momentum distribution resulting in the broader wings of the experimental Compton profile. Inclusion of these electrons in the calculation will improve the comparison and how to do this is discussed next.

The core electrons retain by-and-large their atomic properties. Their contribution to $\mathrm{Im}[1/\epsilon(q,\omega)]$ at $q = 0$ can be estimated based on atomic photoabsorption data as published by Henke et al. [33]. In Ref. [12] it was suggested to separate $\mathrm{Im}[1/\epsilon(q,\omega)]$ in two energy regions: the first region with energy losses smaller than the binding energy of the first core level, the second region for larger energy losses. The contribution of the valence electrons to the dielectric function in the first region is then calculated with Mermin oscillators, and in the second region the loss function is due to contributions from core electrons, which is calculated based on atomic oscillator strengths.

However, for q values large enough for the measurement of a Compton profile the separation of the loss function into two regions fails as both core and valence electrons contribute to the Compton profile. Hence, notwithstanding their atomic nature, it was attempted here to describe the photo-absorption data in terms of Mermin oscillators as well. Using 4 additional oscillators (see Table 1) an approximate description of the loss function in the optical limit was obtained, see Fig. 5.

Table 1
The parameters for the dielectric function as derived here for a Mermin model are given in the first three columns. For comparison the last 3 columns show the parameters obtained with the QUASUS package based on D–L dielectric function as derived in [27]. The last 4 rows are the additional oscillators used to describe the core-level contribution to the loss function, as described in the text.

A_i	ω_i (eV)	γ_i (eV)	A_i	ω_i (eV)	γ_i (eV)
3.85e−2	6.2	2.4	4.2e−2	6.2	2.4
1.30e−1	11	3	1.39e−1	11	3
7.8e−2	14	3	9.1e−2	14	3
8.8e−2	18	7	7.9e−2	18	7
3.36e−1	26.5	10	3.66e−1	27	12
1.6e−2	39.5	3	1.1e−2	39.5	3
9.0e−2	47.5	4.5	5.5e−2	47.5	5.5
4.5e−2	53.5	8	1.28e−1	53.5	17
2.8e−2	90	50	1.26e−2	90	50
4.2e−3	180	150			
6e−4	500	150			
8e−4	700	350			
2e−5	2200	2000			

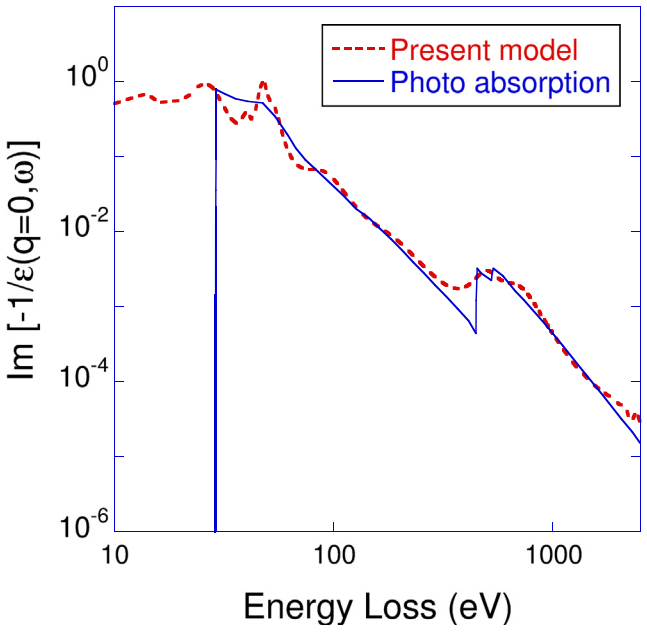

Fig. 5. The modelling of the dielectric function at larger energy losses at $q = 0$ based on the photoabsorption data of Henke et al. [33].

As can be seen in Fig. 4 the Compton profile calculated based on all 13 oscillators compares surprisingly well with the experimental one. The calculated profile was convoluted with the experimental momentum resolution (0.55 a.u.). The theory underestimates the Compton profile near 1.5 a.u. somewhat, but overall considering the crudeness of our model the agreement is quite good.

It turns out that for the full set of oscillators one obtains reasonable values for the Bethe sum rule:

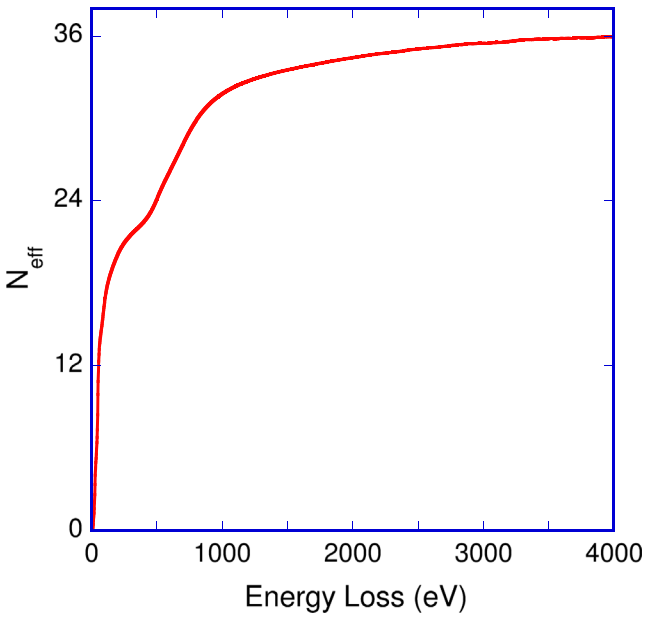

Fig. 6. The result of the Bethe Sum rule. There are 24 electrons in a TiO_2 molecule with binding energies below 100 eV. There are another 12 electrons (O 1s, Ti 2p, 2s, between 400 and 600 eV binding energy).

$$N_{\mathrm{eff}}(\omega) = \frac{1}{2\pi^2 N}\int_0^{\omega} d\omega' \omega' \mathrm{Im}\left[\frac{-1}{\epsilon(q\omega')}\right] \quad (10)$$

with N_{eff} the effective number of electrons that can be excited and N the number of unit cells per unit volume. For ω values well above the binding energy of the valence band N_{eff} should approach the number of valence electrons (24 for TiO_2), and for ω values well above 560 eV N_{eff} should increase by 12 (due to O 1s and Ti 2s and Ti 2p electrons). The resulting values of the Bethe sum rule are given in Fig. 6. Near 5000 eV there should be another increase due to the Ti 1s electrons, but no attempt was made to include these in the model.

It should be noted that stopping powers derived from the present dielectric function are considerably lower than those calculated by Limandri et al., using the related MELF-GOS method [32]. This is not due to the analysis procedure followed, but due to the substantial difference between the calculated energy loss function for TiO_2 [34] used by Limandri et al. and the experimental loss function based on a REELS experiment used here. Note that the loss function as measured by Fuentes et al. [35] for TiO_2 would give even lower stopping power values. Understanding these discrepancies is an outstanding task, and could be related to similar discrepancies between different sets of REELS data as observed for hafnia [36].

5. Conclusion and discussion

Here we have described a method for experimentally obtaining an estimate of the dielectric function of TiO_2 based on REELS and photo-absorption data. The method uses a set of Mermin loss functions. Surprisingly, in this way one obtains a fairly good description of the measured Compton profile, a signature of the loss function in the high momentum transfer limit. The Kramers–Kronig sum rules were used to set the dielectric function on an absolute scale. The resulting dielectric function is in good agreement with the Bethe sum rule.

It is quite remarkable that one obtains a reasonable description of the Compton profile based on a fit of the REELS measurements (for the valence electrons) and photoabsorption measurements (for the core electrons) with a sum of Mermin oscillators. Of course with a limited number of oscillators one can not reproduce the sharp ionisation edges present in the photo-absorption data but by introducing more oscillators this could be accomplished, see e.g. the work by Da et al. [2] for a more precise analysis of the valence band. More surprising is that this method works as well for the core electron contribution, which is modelled here as well in terms of free-electron dielectric functions.

It is tempting to connect the approach here to the local plasma approximation introduced by Lindhard and Scharff [37]. It is discussed at some length by Johnson and Inokuti [38] and Sigmund [39]. In this approximation the stopping of a fast ion near the nuclei is approximated based on the electron density at the position of the ion. The stopping power is assumed to be equal to that of a plasma with the same density. In this model the solid is described as regions with different plasma densities, and each density would have its own Mermin oscillator. Indeed the approaches of Tung et al. [40] and Penn [14] for the description of the energy loss follows this line of argument. The results here give some credence to the use of a set of Mermin loss function for the description of a variety of materials and a wide range of momentum transfers, but the limits of this approach need to be investigated further.

Acknowledgements

This research was made possible by funding of the Australian Research Council. The author wants to thank I. Abril, N. Arista, C. Chantler, P.L. Grande and E Weigold for helpful and stimulating discussions.

References

[1] D. Emfietzoglou, I. Abril, R. Garcia-Molina, I. Petsalakis, H. Nikjoo, I. Kyriakou, A. Pathak, Semi-empirical dielectric descriptions of the bethe surface of the valence bands of condensed water, Nucl. Instrum. Methods Phys. Res. Sect. B: Beam Interact. Mater. Atoms 266 (2008) 1154.
[2] B. Da, H. Shinotsuka, H. Yoshikawa, Z.J. Ding, S. Tanuma, Extended mermin method for calculating the electron inelastic mean free path, Phys. Rev. Lett. 113 (2014) 063201.
[3] C.T. Chantler, J.D. Bourke, Momentum-dependent lifetime broadening of electron energy loss spectra: sum rule constraints and an asymmetric rectangle toy model, Phys. Rev. B 90 (17) (2014).
[4] J.D. Bourke, C.T. Chantler, Momentum-dependent lifetime broadening of electron energy loss spectra: a self-consistent coupled-plasmon model, J. Phys. Chem. Lett. 6 (3) (2015) 314–319.
[5] W. Werner, K. Glantschnig, C. Ambrosch-Draxl, Optical constants and inelastic electron-scattering data for 17 elemental metals, J. Phys. Chem. Ref. Data 38 (2009) 1013–1092.
[6] F. Yubero, J. Sanz, B. Ramskov, S. Tougaard, Model for quantitative analysis of reflection-electron-energy-loss spectra: angular dependence, Phys. Rev. B 9719–9727 (1996).
[7] P.E. Batson, J. Silcox, Experimental energy-loss function, $Im[-\frac{1}{\epsilon}(q,\omega)]$, for aluminum, Phys. Rev. B 27 (1983) 5224–5239.
[8] D.J. Planes, R. Garcia-Molina, I. Abril, N.R. Arista, Wavenumber dependence of the energy loss function of graphite and aluminium, J. Electron Spectrosc. Relat. Phenom. 82 (1996) 23.
[9] R.H. Ritchie, A. Howie, Electron excitation and the optical potential in electron microscopy, Philos. Mag. 36 (1977) 463.
[10] D. Emfietzoglou, F.A. Cucinotta, H. Nikjoo, A complete dielectric response model for liquid water: a solution of the bethe ridge problem, Radiat. Res. 164 (2005) 202.
[11] N. Mermin, Lindhard dielectric function in the relaxation-time approximation, Phys. Rev. B 1 (1970) 2362–2363.
[12] I. Abril, R. Garcia-Molina, C. Denton, F. Pérez-Pérez, N. Arista, Dielectric description of wakes and stopping powers in solids, Phys. Rev. A 58 (1998) 357.
[13] M.J. Cooper, Compton scattering and electron momentum determination, Rep. Prog. Phys. 48 (1985) 415–481.
[14] D. Penn, Electron mean-free-path calculations using a model dielectric function, Phys. Rev. B 35 (1987) 482–486.
[15] J. Ashley, Interaction of low-energy electrons with condensed matter: stopping powers and inelastic mean free paths from optical data, J. Electron Spectrosc. Relat. Phenom. 46 (1988) 199.
[16] C.J. Powell, A. Jablonski, Evaluation of calculated and measured electron inelastic mean free paths near solid surfaces, J. Phys. Chem. Ref. Data 28 (1999) 19.
[17] D. Emfietzoglou, I. Kyriakou, I. Abril, R. Garcia-Molina, H. Nikjoo, Inelastic scattering of low-energy electrons in liquid water computed from optical-data models of the bethe surface, Int. J. Radiat. Biol. 88 (2012) 22.
[18] M. Vos, A.S. Kheifets, E. Weigold, F. Aryasetiawan, Evidence of electron correlation effects in the spectral momentum density of graphite, Phys. Rev. B 63 (2001) 033108.
[19] M. Vos, C. Bowles, A. Kheifets, M. Went, Electron momentum spectroscopy of light and heavy targets, J. Electron Spectrosc. Relat. Phenom. 149 (2005) 20–28.
[20] W.S.M. Werner, Electron transport in solids for quantitative surface analysis, Surf. Interface Anal. 31 (2001) 141.
[21] S. Tanuma, C.J. Powell, D.R. Penn, Calculations of electron inelastic mean free paths. IX. Data for 41 elemental solids over the 50 eV to 30 keV range, Surf. Interface Anal. 43 (2011) 689.
[22] N. Pauly, M. Novák, A. Dubus, S. Tougaard, Comparison between surface excitation parameter obtained from queels and sesinipac, Surf. Interface Anal. 44 (2012) 1147–1150.
[23] <http://esca.atomki.hu/novmis/sesinipac/>. URL sesinipac.
[24] H. Wellenstein, R. Bonham, R. Ulsh, Bethe surface and inelastic and elastic differential cross sections for helium obtained by use of 25-keV incident electrons, Phys. Rev. A 8 (1973) 304.
[25] B.G. Williams, T.G. Sparrow, R.F. Egerton, Electron Compton scattering from solids, Proc. Roy. Soc. A 393 (1984) 409–422.
[26] Z. Feng, S. Löffler, Eder D. Su, J. Meyer, P. Schattschneider, Combined study of the ground and unoccupied electronic states of graphite by electron energy-loss spectroscopy, J. Appl. Phys. 114 (2013) 183716.
[27] M. Vos, P. Grande, High-energy electron scattering from TiO_2 surfaces, Nucl. Instrum. Methods B 354 (2015) 332.
[28] S. Tougaard, I. Chorkendorff, Differential inelastic electron scattering cross sections from experimental reflection electron-energy-loss spectra: application to background removal in electron spectroscopy, Phys. Rev. B 35 (1987) 6570–6577.
[29] A. Gupta (Ph.D. thesis), University of Rajasthan, Jaipur, India, 1987.
[30] F. Yubero, S. Tougaard, Quantitative analysis of reflection electron energy-loss spectra, Surf. Interface Anal. 19 (1992) 269–273.

[31] R.F. Egerton, Electron Energy-loss Spectroscopy in the Electron Microscope, Plenum Press, New York, 1996.
[32] S. Limandri, R. Fadanelli, M. Behar, L. Nagamine, J. Fernandez-Varea, I. Abril, R. Garcia-Molina, C. Montanari, J. Aguiar, D. Mitnik, J.E. Miraglia, N. Arista, Stopping cross sections of TiO_2 for H and He ions, Eur. Phys. J. D 68 (2014) 194.
[33] B. Henke, E. Gullikson, J. Davis, X-ray interactions: photoabsorption, scattering, transmission, and reflection at e = 50–30,000 eV, z = 1–92, At. Data Nucl. Data Tables 54 (1993) 181.
[34] L. Dash, F. Bruneval, V. Trinité, N. Vast, L. Reining, Electronic excitations: ab initio calculations of electronic spectra and application to zirconia ZrO_2, titania TiO_2 and cuprous oxide Cu_2O, Comput. Mater. Sci. 38 (2007) 482.
[35] G.G. Fuentes, E. Elizalde, F. Yubero, J.M. Sanz, Electron inelastic mean free path for Ti, TiC, TiN and TiO_2 as determined by quantitative reflection electron energy-loss spectroscopy, Surf. Interface Anal. 33 (2002) 230.
[36] M. Vos, P. Grande, The relation between the electron energy loss spectra of hafnia and its dielectric function, Surf. Sci. 630 (2014) 1–8.
[37] J. Lindhard, M. Scharff, Energy loss in matter by fast particles of low charge, Mat. Fys. Medd. Dan. Vid. Selsk. 27 (1953) 15.
[38] R. Johnson, M. Inokuti, The local-plasma approximation to the oscillator-strength spectrum: how good is it and why?, Commun At. Mol. Phys. 14 (1983) 19.
[39] P. Sigmund, Particle Penetration and Radiation Effects, Springer Series in Solid-state Sciences, vol. 151, Springer, Berlin, 2006.
[40] C. Tung, J. Ashley, R. Ritchie, Electron inelastic mean free paths and energy losses in solids II: electron gas statistical model, Surf. Sci. 81 (2) (1979) 427.